Applied Catalysis B: Environmental 180 (2016) 434–441

Contents lists available at ScienceDirect

Applied Catalysis B: Environmental

journal homepage: www.elsevier.com/locate/apcatb

Catalytic activity of $Fe_{3-x}Cu_xO_4$ ($0 \leq x \leq 0.25$) nanoparticles for the degradation of Amaranth food dye by heterogeneous electro-Fenton process

Willyam R.P. Barros[a], Juliana R. Steter[b], Marcos R.V. Lanza[b,*], Ana C. Tavares[a,*]

[a] Institut National de la Recherche Scientifique—Énergie, Matériaux et Télécommunications, 1650 Boulevard Lionel-Boulet, Varennes, QC J3X 1S2, Canada
[b] Instituto de Química de São Carlos, Universidade de São Paulo, Avenida Trabalhador São Carlense 400, São Carlos, 13566-590 SP, Brazil

ARTICLE INFO

Article history:
Received 20 March 2015
Received in revised form 12 June 2015
Accepted 24 June 2015
Available online 30 June 2015

Keywords:
Heterogeneous electro-Fenton
Gas diffusion electrode
$Fe_{3-x}Cu_xO_4$ nanoparticles
Alkaline medium

ABSTRACT

This work describes the application of substituted magnetite nanoparticles, $Fe_{3-x}Cu_xO_4$ ($0 \leq x \leq 0.25$), as heterogeneous catalysts for the electro-Fenton process in alkaline medium (KOH, pH 13.4) using an uncatalyzed gas diffusion electrode based on Printex carbon. The, $Fe_{3-x}Cu_xO_4$ ($0 \leq x \leq 0.25$) nanoparticles were synthesized by a co-precipitation method and were characterized by neutron activation analysis (NAA), X-ray diffraction (XRD), transmission electron microscopy (TEM), N_2-physisorption analysis and X-ray photoelectron spectroscopy (XPS). Cu^{2+}/Cu^{+} cations were successfully substituted in the octahedral site of Fe_3O_4 causing changes in the catalytic activity of the NPs. The electrodegradation of amaranth food dye was performed at −1.1 V (*vs.* Ag/AgCl) for 90 min under constant flow of O_2 in the GDE. The dye solution samples were analyzed by UV–vis spectrophotometry, high performance liquid chromatography (HPLC) and total organic carbon (TOC). The maximum color removal was 98%, the degradation was 98%, the mineralization was 70% and the specific energy consumption 483.0 kWh kg^{-1} for $Fe_{3-x}Cu_xO_4$ with $x = 0.25$. The kinetics of the process was of pseudo-first order. The consumed H_2O_2 increased with increasing value of x in the spinel of $Fe_{3-x}Cu_xO_4$ ($0 \leq x \leq 0.25$). No residues of soluble Fe^{2+} and Cu^{2+} ions were detected at the end of electrolysis. XRD analysis of the $Fe_{2.75}Cu_{0.25}O_4$ (limit of the solid solution) confirmed the stability of the NPs after the Fenton test.

1. Introduction

Technological development contributes to the disposal of increasing amounts of waste and toxic compounds in several types of effluents. These wastes are contaminants of the aquatic biota, decreasing the amount of dissolved oxygen and modifying the properties and characteristics of water courses, affecting hydric resources [1–3]. Thus, awareness of the need to avoid such contaminations in the environment has further reinforced the search for effective methods and new solutions that promote the complete removal of these contaminants from wastewater.

Synthetic organic dyes are heavily used in textile industry and as additives in food industry. Many synthetic dyes and their derivatives, especially aromatic amines and phenol compounds are harmful to environment, i.e., may cause problems such as changes in water color, odor, eutrophication and bioaccumulation [4,5]. Some of the available treatments for wastewater contaminated with dyes consist in the use of microorganisms and biosorption direct systems [6–8], or adsorption using various inorganic compounds [9–12]. However, these processes are not effective with respect to total removal of dyes and their intermediates.

Advanced oxidation process (AOP) is an alternative technology that has been applied for the remediation of wastewater containing dyes [13–15], and other organic pollutants [16–18], showing good performance in terms of discoloration and degradation. The electro-Fenton (E-Fenton) process stands out among the various types of AOP, as one of the most efficient technologies for the oxidation of wastewater contaminated by dyes [19–21]. It is based on the generation of a powerful oxidizing radical (hydroxyl radical, •OH) in aqueous solution by reaction between electrogenerated hydrogen peroxide (H_2O_2) and iron ions as catalyst (Eqs.1–3) [22,23].

$$Fe^{2+} + H_2O_2 \rightarrow Fe^{3+} + HO^- + {}^{\bullet}OH \quad k = 63.0\ mol\ L^{-1}\ s^{-1} \quad (1)$$

$$Fe^{3+} + H_2O_2 \rightarrow Fe^{2+} + H^+ + {}^{\bullet}O_2H \quad k = 8.4\ mol\ L^{-1}\ s^{-1} \quad (2)$$

$$Fe^{3+} + {}^{\bullet}O_2H \rightarrow Fe^{2+} + H^+ + O_2 \quad k = 2 \times 10^3\ mol\ L^{-1}\ s^{-1} \quad (3)$$

* Corresponding authors. Fax: +1 450 9298102.
E-mail addresses: marcoslanza@iqsc.usp.br (M.R.V. Lanza), tavares@emt.inrs.ca (A.C. Tavares).

http://dx.doi.org/10.1016/j.apcatb.2015.06.048
0926-3373/

Table 1
Bulk and surface composition of the nanoparticles.

x	at% Cunominal	at% Cubulk[1]	at% Cu/at% Fenominal	at% Cu/at% Fesurface[2]
0.05	1.3	1.2	0.017	0.093
0.10	2.7	2.2	0.034	0.163
0.25	6.8	6.0	0.091	0.232

[1] From neutron activation analysis.
[2] Determined using the area under the main peaks of the Cu ($2p_{3/2}$) and Fe ($2p_{3/2}$) and respective SF factors.

One of the many advantages of the homogeneous E-Fenton process relative to the traditional chemical Fenton process is the higher rate of degradation of the organic pollutants due to the continuous regeneration of Fe^{2+} at the cathode. However, the process is limited to an operative pH between 2.0 and 3.5 to avoid the precipitation of iron ions in the form of iron hydroxide causing the formation of a sludge [5,23].

Heterogeneous catalysts based on iron oxide nanoparticles (NPs) have been used to circumvent the pH limitation of the E-Fenton process [24–27]. The iron ions are immobilized on the surface of the catalyst and are not subjected to a complexation reactions at high pH [24–26]. In particular, magnetite (Fe_3O_4) is considered as an efficient heterogeneous catalyst and has been used in the oxidation of several organic compounds via the Fenton process [27–31]. Its activity was related to the existence of both Fe^{2+} and Fe^{3+} ions in the octahedral site of its crystal structure, which activate the decomposition of the H_2O_2 molecule leading to the formation of $^{\bullet}OH$ radicals [32,33]. Meanwhile, its inherent magnetism makes easy the separation of the NPs from the reactional system at the end of the operation [34].

To minimize the consumption of energy and to implement the heterogeneous E-Fenton process as a cost effective process, the kinetic of degradation of organic compounds by $^{\bullet}OH$ generated *in situ* should be high. Thus, the design and synthesis of novel nanostructured heterogeneous catalysts are of paramount importance. In this sense, several studies reported in the literature have demonstrated the importance of the co-existence of $M^{n+}/M^{(n+1)+}$ redox pairs in the octahedral sites of the spinel structure to promote the generation of peroxide radicals and to increase the efficiency of the oxidation of organic compounds. Indeed, it was demonstrated in literature that the use of elements like Co, Cr, Mn and V in spinel systems of the type $Fe_{3-x}Co_xO_4$ [35,36], $Fe_{3-x}Cr_xO_4$ [37], $Fe_{3-x}Mn_xO_4$ [35,36] and $Fe_{3-x}V_xO_4$ [38] promote the oxidation rate of toxic organic molecules during the heterogeneous Fenton process. In addition, it was also demonstrated that often the formation of substitutional solid solutions is accompanied by an increase of the specific surface area (SSA) of the NPs [38–40]. This not only facilitates the adsorption on dye on the surface of the NPs but also increases the $H_2O_2/^{\bullet}OH$ conversion due to a higher number of exposed active sites.

To the best of our knowledge no studies were reported in the literature concerning the use of $Fe_{3-x}Cu_xO_4$ NPs for the degradation of organic molecules by the Fenton process. It is well known that spinel oxides can easily accommodate copper ions on the crystallographic structure [41–45]. Brillas et al. [46] reported that the Cu^{2+}/Cu^{+} couple had a low catalytic activity for the homogeneous E-Fenton process, however the Cu^{2+} ions showed catalytic activity when combined with the Fe^{2+} or Fe^{3+} ions. Therefore it is interesting to verify if similar effect occurs with heterogeneous catalysts.

This work aims at verifying the potential use of $Fe_{3-x}Cu_xO_4$ ($0 \leq x \leq 0.25$) NPs for the E-Fenton process in alkaline solution. High specific surface area NPs were synthesized using a simple co-precipitation method, and the influence of their surface properties on the efficiency of the process analyzed. The H_2O_2 was electrogenerated *in situ* using KOH 1 mol L^{-1} (pH 13.4) as electrolyte and an uncatalyzed gas diffusion electrode (GDE) based on Printex carbon. As we shown recently, at this pH a very high concentration of H_2O_2 can be electrogenerated *in situ* (3370 mg L^{-1} of H_2O_2 electrogenerated *vs.* 176 mg L^{-1} in acid electrolyte at optimized potentials) [47]. Amaranth (AM) food dye was chosen to test the catalytic activity of the NPs during the electrodegradation process.

2. Experimental

2.1. Chemicals and materials

Amaranth food dye (AM) (85–95% purity), sodium bisulfite (58.5%), phenanthroline (99.0%), iron (II) chloride (98.0%), iron (III) chloride (99.0%), copper (II) chloride (99.9%) and sodium borohydride (98.8%) were purchased from Sigma Aldrich. Potassium hydroxide (85.0%), ammonium acetate (98.0% analytical grade) and ethylenediaminetetraacetic acid (EDTA, 99.0%) were purchased from Synth. Methanol (HPLC grade) was purchased from Merck and sodium hydroxide (95.0%) was purchased from Fischer. For the preparation of all solutions was used ultrapure water (Millipore Milli-Q 18 MΩ cm^{-1}).

$Fe_{3-x}Cu_xO_4$ ($0 \leq x \leq 0.25$) NPs were synthesized by a modified co-precipitation method that we proposed in a previous work for the synthesis of Fe_3O_4 NPs [48]. Briefly, stoichiometric amounts of $FeCl_2.4H_2O$, $FeCl_3.6H_2O$ and $CuCl_2.H_2O$ were dissolved in deionized water and a solution of $NaBH_4$ (reducing agent) was carefully added. NaOH solution was then added to precipitate the NPs and this step was carried out at 90 °C. The NPs were collected from the solution with a magnet and dried at 100 °C for 3 h. All steps were carried out under a continue flow of N_2.

2.2. Characterization of $Fe_{3-x}Cu_xO_4$ ($0 \leq x \leq 0.25$) NPs

The bulk Cu content was verified by Neutron Activation Analysis (NAA, SLOWPOKE Laboratory at École Polytechnique de Montreal), Table 1. The error in the chemical analysis is ±5 wt.% for the element concentration.

X-ray diffraction (XRD) analysis of the NPs was carried out using a Bruker D8 Advance X-ray diffractometer equipped with CuKα source (λ = 1.5406 Å) operating at 40 kV and 40 mA. The angular range was comprised between 2–80° in 2θ, the step mode was 0.01° in 2θ and 8s duration. The cell parameter (a) values were calculated using EVA V14 software.

Transmission electron microscopy (TEM) analysis was carried out with a Transmission Electron Microscope JEOS-2100F operating at 200 kV (Center for Characterization of Microscopic Materials, at Ecole Polytechnique de Montreal). The TEM samples were prepared by dipping copper grids into dispersions of the powders in methanol in the case of Fe_3O_4 powders, and Lacey carbon grids in the case of the $Fe_{3-x}Cu_xO_4$ (x = 0.05, 0.10, 0.25) samples.

N_2-physisorption analyses were performed using Quantachrome Instrument Autosorb-1 and the isotherms were recorded at −196 °C. The NPs were weighed, placed on the analysis port, and prior to analysis they were heated at 200 °C for 2 h under vacuum. The specific surface area data was obtained using the BET theory.

X-ray photoelectron spectroscopy (XPS) spectra were registered on a VG Escalab 220i-XL using polychromatic Mg Kα ($h\nu$ = 1253.6 eV) from an X-ray source operating at 15 kV and 20 mA. The analyzer pass energy was 20 eV and the energy step size was

0.1 eV for all elements. The C (1s) photoelectron peak binding energy (284.5 eV) was used as an internal standard for the correction of the charging effect in all NPs samples. The casa XPS version 2315 software was used to calculate the elemental concentrations.

2.3. Electrochemical oxidation of the AM dye by heterogeneous E-Fenton process

The electrodegradation of the AM dye was carried out in single compartment electrochemical cell equipped with the working electrode (unmodified Printex based gas diffusion electrode), reference electrode (Ag/AgCl), counter electrode (Pt screen), and constant mechanical stirring. The gas diffusion electrode (GDE) was prepared according to the literature [49,50]. The cell was filled with 400 mL of an aqueous solution 100 mg L^{-1} of AM dye in 1 mol L^{-1} KOH (pH 13.4), and 0.15 mmol of the $Fe_{3-x}Cu_xO_4$ ($0 \le x \le 0.25$) NPs were added to the solution. The study was done at controlled temperature (20 °C). The GDE was pressurized with O_2 gas under 0.2 bar gauge pressure and the *in situ* electrogeneration of H_2O_2 was conducted at −1.1 V (*vs.* Ag/AgCl) for 90 min. According to a previous study, the H_2O_2 electrogenerated at −1.1 V (*vs.* Ag/AgCl) was 3370 mg L^{-1} [47].

All tests of the AM dye degradation were performed using a potentiostat/galvanostat PGSTAT-302 (AUTOLAB) with high current module (10A-BSTR) and a multimeter placed in parallel with the working and counter electrodes was used to measure the cell potential (E_{cell}).

Samples were collected at appropriate periods of time after the beginning of the electrolysis, and immediately treated with an aqueous solution of sodium bisulfite to convert the residual H_2O_2 to the H_2O and SO_4^{2-} (Eqs. 4–6), thus preventing any further oxidation of the dye.

$$2H_2O_2 \rightarrow 2H_2O + O_2 \quad (4)$$

$$2SO_3 + O_2 \rightarrow 2SO_4^{2-} \quad (5)$$

$$2H_2O_2 + 2SO_3 \rightarrow 2H_2O + 2SO_4^{2-} \quad (6)$$

2.4. Analytical methods

The discoloration rate related to the formation of non colored intermediates of AM dye was monitored at 521 nm by Agilent Varian Cary-50 UV–vis spectrophotometer.

The percentage of discoloration was obtained from Eq. (7), where $Abs_{(Dye)\ t}$ and $Abs_{(Dye)\ 0}$ are the absorbance at time t and 0 min, respectively.

$$\text{Discoloration}\ (\%) = 1 - \left(\frac{Abs_{(DYE)_t}}{Abs_{(DYE)_0}}\right) \times 100 \quad (7)$$

The concentration of AM during the degradation process was quantified by high performance liquid chromatograph (HPLC), using a Shimadzu LC-20AT chromatograph coupled with a SPD-20A diode array detector and a Phenomenex Luna C_{18} column (250 × 4.6 mm i.d.) maintained at 25 °C. The mobile phase used was a mixture in the ratio of 30:70 (v/v) of methanol and an aqueous solution of 0.08 mol L^{-1} ammonium acetate employing isocratic elution supplied at a flow rate of 0.5 mL min^{-1}. The used detection wavelength was 260 nm and the dye concentration was determined by referring to a calibration curve built using analytical standards of AM. The percentage in the degradation of the AM dye ($C_{(Dye)}$) was calculated by Eq. (8).

$$\text{Degradation}\ (\%) = 1 - \left(\frac{C_{(DYE)_t}}{C_{(DYE)_0}}\right) \times 100 \quad (8)$$

The mineralization of the AM dye to CO_2 and H_2O was determined using a Shimadzu model TOC-VCPN PC-controlled TOC analyzer.

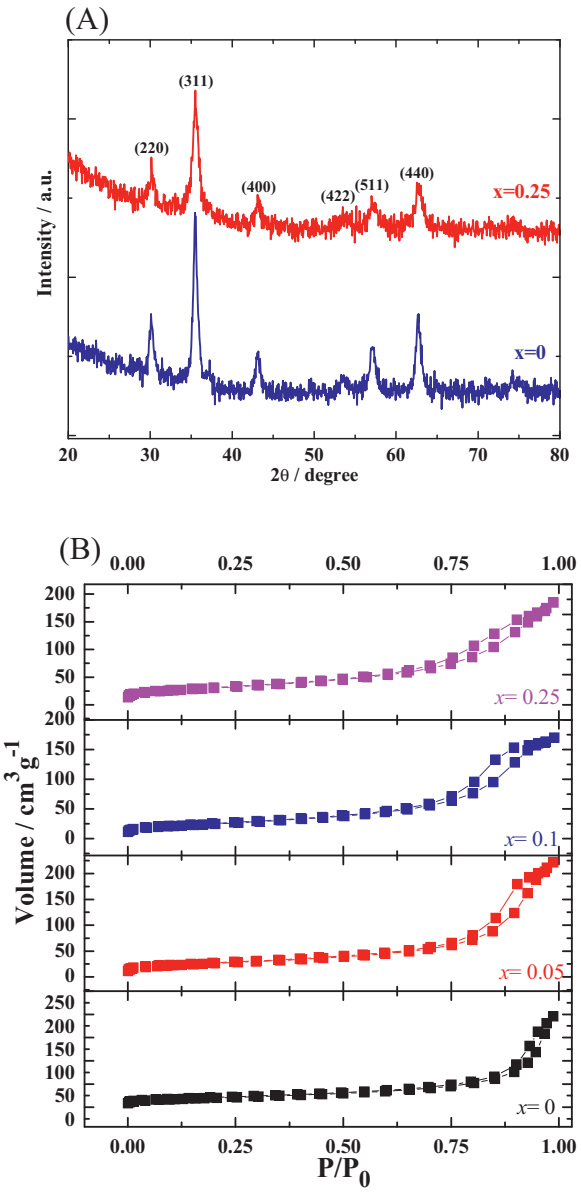

Fig. 1. (A) XRD patterns of $Fe_{3-x}Cu_xO_4$ with $x = 0$ and 0.25 and (B) N_2 sorption isotherms of $Fe_{3-x}Cu_xO_4$ ($0 \le x \le 0.25$) nanoparticles.

The H_2O_2, Fe^{2+}, $Fe^{3+}$and Cu^{2+} residual concentrations at the end of the electrolysis were quantified spectrophotometrically by a Varian Cary-50 UV–vis spectrophotometer. The residual and consumed H_2O_2 were quantified at $\lambda = 350$ nm using the peroxymolybdate method as described in a previous work [47]. The determination of residual Fe^{2+} and Fe^{3+} ions ($\lambda = 510$ nm) was done using the phenanthroline colorimetric method recommended by the American Public Health Association [51]. The EDTA-Cu^{2+} complexometric method ($\lambda = 745$ nm) [52] was used to verify the presence of Cu^{2+} ions present in the dye solution after the electrolysis.

3. Results and discussion

3.1. Characterization of $Fe_{3-x}Cu_xO_4$ ($0 \le x \le 0.25$) nanoparticles

The X-ray diffraction (XRD) of Fe_3O_4 and $Fe_{2.75}Cu_{0.25}O_4$ are presented in Fig. 1A. Similar diffractograms were recorded for $x = 0.05$ and 0.10. The characteristic peaks of Fe_3O_4 cubic spinel structure (JCPDS #19-0629) were identified in all diffractograms suggest-

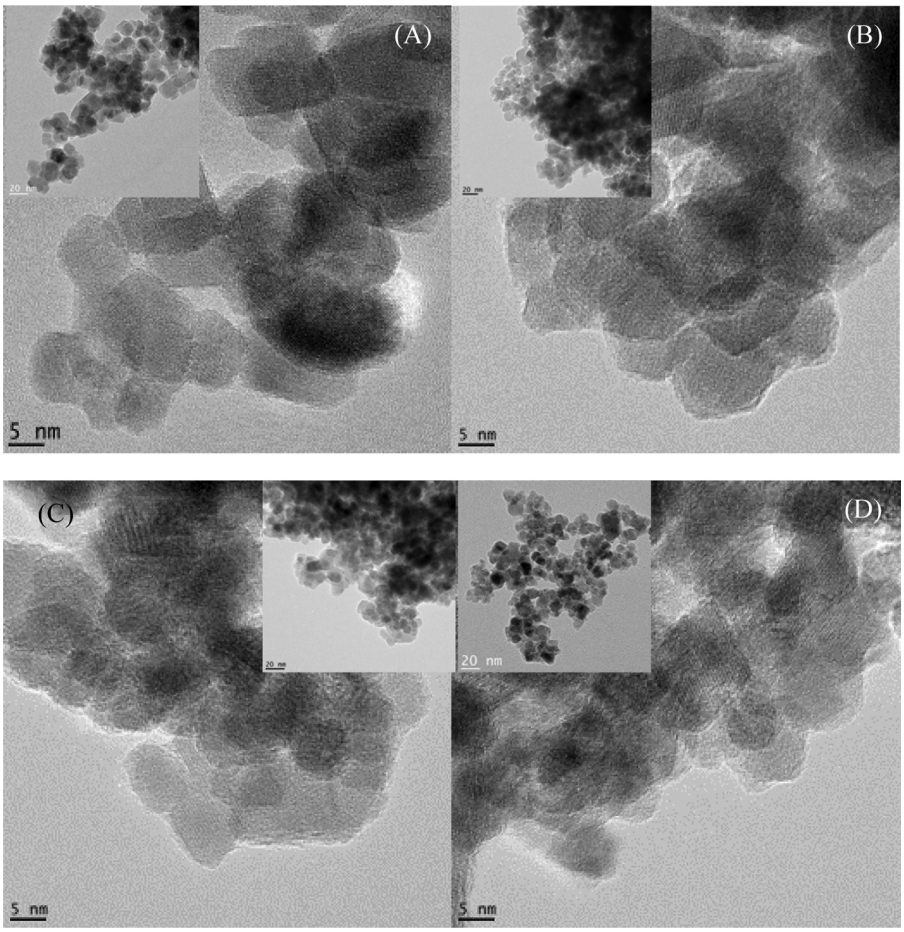

Fig. 2. TEM images of (A) Fe_3O_4, (B) $Fe_{2.95}Cu_{0.05}O_4$, (C) $Fe_{2.9}Cu_{0.1}O_4$ and (C) $Fe_{2.75}Cu_{0.25}O_4$ nanoparticles.

ing the formation of substitutional solid solutions for $x \leq 0.25$. The lattice parameter calculated from (3 1 1) crystalline plane was $a = 8.397$ Å for Fe_3O_4 and decreased to 8.374 Å as the copper content increased to $x = 0.25$. The decrease of a with increasing x is consistent with the partial replacement of Fe^{2+} ions by Cu^{2+} ions in the octahedral sites of the spinel structure. In fact, Cu^{2+} ions have higher preference for the octahedral sites [53,54] and a lower ionic radius (0.73 Å for Cu^{2+} *vs.* 0.78 Å for Fe^{2+} in octahedral coordination) with respect to Fe^{2+} ions [55]. NPs with nominal composition $x = 0.50$ were also synthesized. However the diffraction peaks of CuO could be clearly seen in the diffractograms indicating that this composition was above the limit of formation of $Fe_{3-x}Cu_xO_4$ substitutional solid solution.

The specific surface area (SSA) of the NPs determined through N_2-physisorption analysis (isotherms shown in Fig. 1B and zoom at low P/P_0 in Fig. SI.1), increased steadily from 70.0 $m^2\,g^{-1}$ for $x = 0$–106.5 $m^2\,g^{-1}$ for $x = 0.25$. A closer inspection of the isotherms reveals the development of microporous (from the initial uptake at low P/P_0) and mesoporous (from the hysteresis loop at intermediate / high P/P_0) features with increasing copper content. According to the IUPAC classification [56] this type of hysteresis loop is indicative of a poorly defined pore system within the NPs. In fact, the TEM images shown in Fig. 2 reveal that the catalysts are formed by single NPs with an average size that decreases from ~20 nm for $x = 0$ to ~5 nm for $x = 0.25$. Interestingly the surface roughness of the NPs increases with x and it could be the origin of the microporous features in the isotherms. The NPs containing copper appear more agglomerated than the Fe_3O_4 NPs leading probably to the poorly defined pore system revealed in the N_2-sorption isotherms.

XPS analysis was used to investigate the surface composition of the NPs and the oxidation states of the Cu species. Representative Fe (2p) and O (1s) spectra are presented in Fig. SI.2. Fig. 3 shows the Cu ($2p_{3/2}$) high resolution spectra registered for $x = 0.05$, 0.10 and 0.25. The satellite band in the Cu ($2p_{3/2}$) spectra indicates the presence of paramagnetic species, namely Cu^{2+} ions. The resolution of the main peak reveals the presence of two copper species. According to the data in the literature concerning $NiCo_{2-y}Cu_yO_4$ and $Ni_{1-x}Cu_xCo_2O_4$ oxides [41], the peaks at *ca.* 933.4 eV can be identified as Cu^{2+} ions in octahedral coordination and the peak at *ca.* 932.2 eV as Cu^{+} ions. The existence of Cu^{+} ions on the surface of spinel oxides was reported before [41,57,58]. Table 1 reports the (Cu/Fe) atomic ratio determined by XPS. The data shows that there is a strong segregation of copper species to the surface of the NPs, as often observed on copper spinel oxides [41–45,57,58], and that this enrichment increases with x.

3.2. Degradation of the AM food dye by heterogeneous E-Fenton process

3.2.1. Kinetic study by UV–vis and HPLC

The discoloration of the AM dye solution by the E-Fenton process in the presence of the NPs was quite effective as shown in Fig. SI.3. The percentage of color removal after 90 min. of treatment was 70% when electrogenerated H_2O_2 only was used. However, when the NPs were added to the solution, the color removal was around 80% and 98% for $x = 0$ and $x = 0.25$, respectively. The observation of a linear relation between $-\ln (C_{DYE})_t/(C_{DYE})_0$ and the electrolysis time, indicates that the discoloration follows a kinetic of pseudo-first order and the values of the apparent rate constant (k_{app}) can

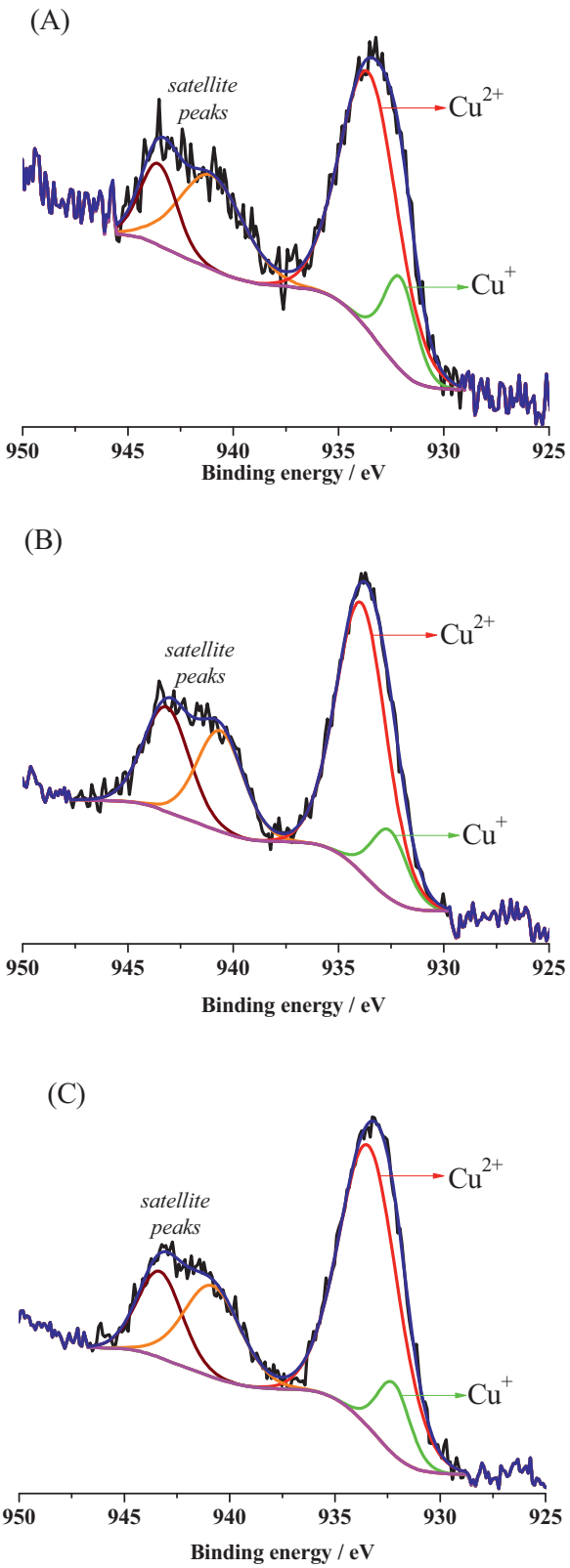

Fig. 3. Cu ($2p_{3/2}$) XPS spectra of (A) $Fe_{2.95}Cu_{0.05}O_4$, (B) $Fe_{2.9}Cu_{0.1}O_4$ and (C) $Fe_{2.75}Cu_{0.25}O_4$ nanoparticles.

be calculated. As shown in Fig. 4A, the k_{appDIS} values follow the same trend of the color removal, *i.e.* the k_{appDIS} value is the lowest when only electrogenerated H_2O_2 is used (1.1×10^{-2} min^{-1}), and in the presence of the NPs it increases from 1.5×10^{-2} min^{-1} ($x = 0$) to 4.0×10^{-2} min^{-1} ($x = 0.25$). These k_{appDIS} values are higher than those reported previously by Barros et al. [20] for homogeneous E-Fenton in acid medium using the same setup: the k_{appDIS} value was 5.7×10^{-3} min^{-1} with electrogenerated H_2O_2 only, and 1.1×10^{-2} min^{-1} with 0.15 mmol of $FeSO_4{\cdot}7H_2O$. The present study confirms that there is notable acceleration of the AM dye degradation in alkaline medium with respect to acid medium, with or without the presence of $Fe_{3-x}Cu_xO_4$ ($0 \leq x \leq 0.25$) NPs.

Dyes containing azo bonds can be anodicaly oxidized or reduced at the cathode [20]. So, in order to verify the influence of these electrochemical processes in the AM dye discoloration process without H_2O_2 electrogeneration, an electrolysis test was conducted without any NPs suspended in the electrolyte and with the GDE pressurized with N_2. The KOH electrolyte was also purged for 45 min. and saturated with N_2 during the electrolysis. From the obtained data, it was found that AM dye discoloration was only 22% after 90 min. (Fig. SI.4B) of electrolysis. It should be mentioned that in spite of purging the electrolyte and feeding the GDE with N_2, electrogenerated H_2O_2 was detected during this electrolysis (maximum amount $\approx$3 mg L^{-1}). This was probably due to the incorporation of a small fraction of O_2 into the electrolyte due to mechanical stirring of the solution during the test.

The degradation of the AM over time was monitored by HPLC. Fig. SI.5A shows the chromatograms recorded before the electrochemical treatment, after 90 min. of electrogeneration of H_2O_2 alone and in the presence of the $Fe_{3-x}Cu_xO_4$ ($0 \leq x \leq 0.25$) NPs. The decrease in the intensity of the peak corresponding to the AM dye (peak at 6 min. of retention time) is quite accentuated in all cases, but as anticipated by the discoloration data, the highest decrease occurs in the presence of the NPs. The concentration of AM dye decreases by 72% when only electrogenerated H_2O_2 is used, by 87% in the presence of Fe_3O_4 NPs, reaching 98% for $x = 0.25$ as shown in Fig. SI.5B. Other peaks at different retention times (*ca.* 4.6, 5.7 and 6.4 min.) appear in the chromatogram of AM dye solution. According to literature, theses peaks suggest the formation of degradation by-products probably following a path similar to those reported previously [14,20]. Accordingly, the AM degradation would begin with the formation of two primary amines and the azoic bond rupture, followed by the attack from •OH radicals and subsequent decarboxylation and hydroxylation processes. After successive steps, occurs the opening of the aromatic ring and aliphatic acids are formed as by-products and subsequent formation of CO_2 and H_2O [13,14].

The linear relationship between ln [dye concentration (mg L^{-1})] and electrolysis time (min), indicates that the decrease in concentration follows a pseudo-first-order kinetic. The variation of k_{appDEG} with the NPs composition is shown in Fig. 4B. The k_{appDEG} was 1.8×10^{-2} min^{-1} for the degradation process using electrogenerated H_2O_2 only. However, the k_{appDEG} values were higher when the NPs were used and increased from 2.3×10^{-2} min^{-1} ($x = 0$) to 4.2×10^{-2} min^{-1} ($x = 0.25$). Using the same electrochemical cell, the literature reports that k_{appDEG} achieved maximum value of 7.2×10^{-3} min^{-1} and 2.5×10^{-2} min^{-1} for the AM degradation by homogeneous E-Fenton process in acid solution with electrogenerated H_2O_2 only and with 0.15 mmol of $FeSO_4{\cdot}7H_2O$, respectively [20]. The k_{appDIS} values are slightly lower than the k_{appDEG} values which indicates the formation of colored products during the degradation process.

As discussed above, the isostructural substitution of Fe by Cu in the $Fe_{3-x}Cu_xO_4$ spinel structure, results in NPs with higher SSA, and strong segregation of Cu^{2+} and Cu^+ ions to the surface. In an attempt to discriminate between geometric and redox effects on

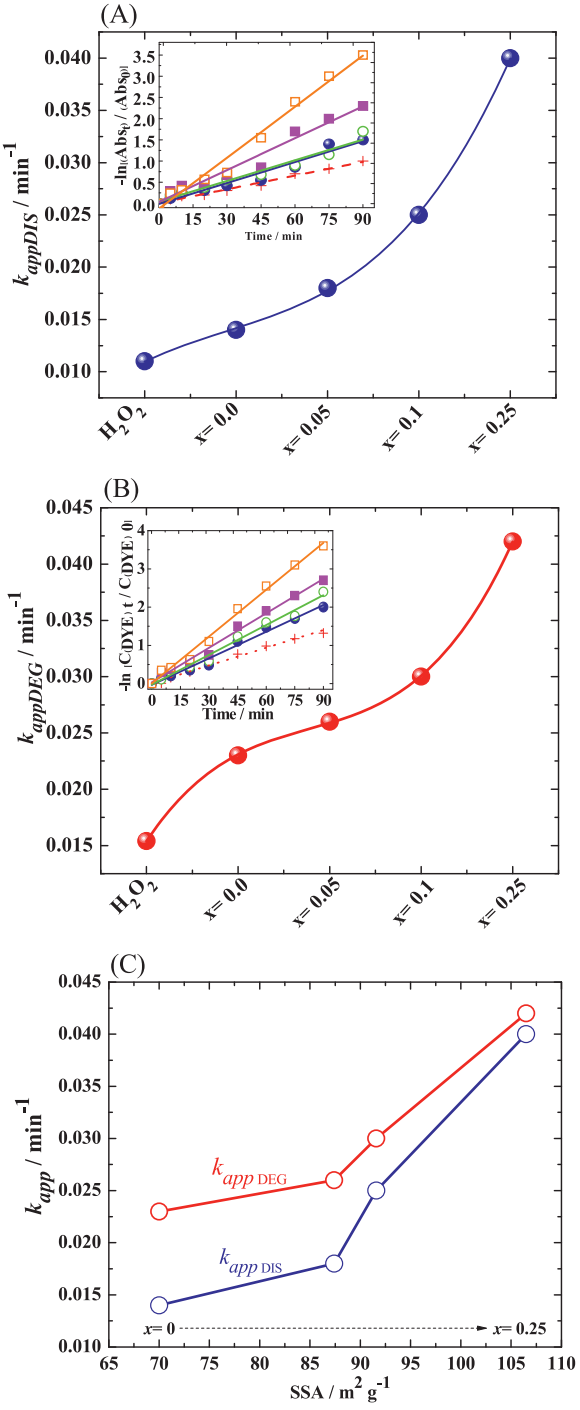

Fig. 4. Apparent rate constants for (A) discoloration (k_{appDIS}) and (B) AM dye degradation (k_{appDEG}) using electrogenerated H_2O_2 and as a function of the $Fe_{3-x}Cu_xO_4$ nanoparticles nominal composition (x). Insets: linear regressions (A) $-\ln(Abs_{DYE})_t/(Abs_{DYE})_0$ versus time of electrolysis and (B) $-\ln(C_{DYE})_t/(C_{DYE})_0$ versus time of electrolysis. (C) Discoloration and decay concentration apparent rate constants as function of specific surface area. Electrogenerated H_2O_2 (. . .+. . .), $x = 0$ (●), $x = 0.05$ (○), $x = 0.1$ (■) and $x = 0.25$ (□).

the kinetic of AM dye degradation, the values of k_{appDIS} and k_{appDEG} were plotted against the SSA of the NPs. As shown in Fig. 4C, the kinetic constants increase with the SSA but the data points do not fall on a single straight line. The inflexion point at $x = 0.05$ indicates that the presence of Cu^{2+}/Cu^{+} surface species promotes in a remarkable way the degradation of the AM dye.

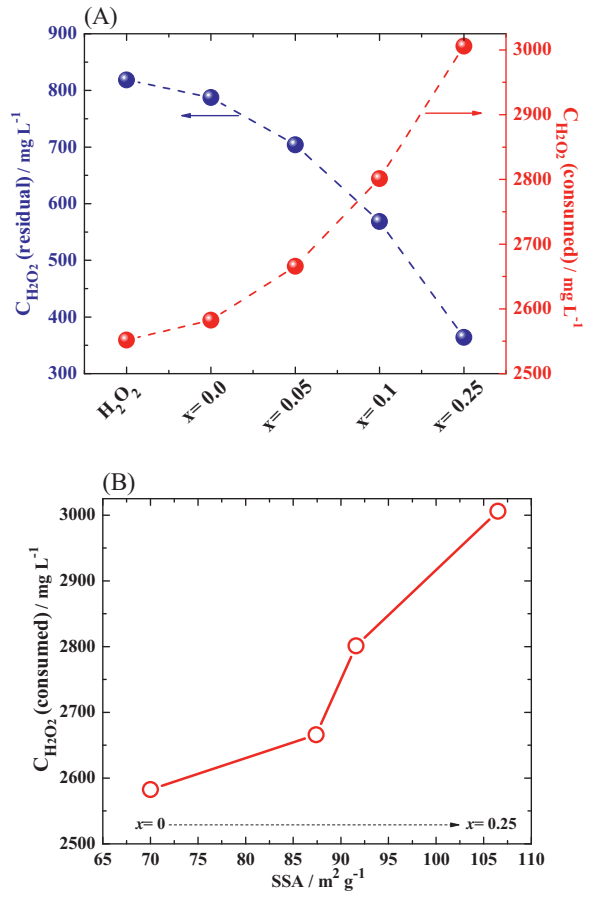

Fig. 5. (A) Residual and consumed H_2O_2 concentration after 90 min. of AM dye degradation using electrogenerated H_2O_2 and $Fe_{3-x}Cu_xO_4$ ($0 \le x \le 0.25$) nanoparticles and (B) consumed H_2O_2 concentration as function of the nanoparticles specific surface area.

The amount of consumed H_2O_2 during the AM dye degradation under heterogeneous conditions was also quantified. Data for the residual and consumed H_2O_2 concentrations are reported in Fig. 5A. The consumed H_2O_2 is the difference between the total amount of electrogenerated H_2O_2 (3370 mg L^{-1}) [47] and the amount of H_2O_2 measured after 90 min. of electrolysis. As show in the Fig. 5A the residual H_2O_2 (818.6 mg L^{-1}) in the absence of NPs was the highest of the series. This can be explained by the fact that H_2O_2 is converted to HO^{2-} ions in alkaline solution, which results in a lower H_2O_2/•OH conversion efficiency [4]. However, the residual H_2O_2 concentration decreased progressively with increasing x, or in other words, the H_2O_2/•OH conversion was accelerated. In fact, for $x = 0.25$, the residual and consumed H_2O_2 concentrations were 364.1 mg L^{-1} and 3005.9 mg L^{-1}, respectively, meaning that 89.2% of H_2O_2 was used in the AM dye oxidation. The consumed H_2O_2 was also plotted against the SSA of the NPs, Fig. 5B. Once again it can be concluded that the Cu^{2+}/Cu^{+} surface species play a fundamental role in enhancing the efficiency of the AM dye degradation.

In fact, the increase of copper content in the NPs led to a growing number of active sites, due to the systematic increase of the NPs' SSA and their surface enrichment with Cu^{2+}/Cu^{+} ions. As the octahedral sites are almost exclusively those exposed on the surface of the Fe_3O_4 spinel [42–45], Cu^{2+}/Cu^{+} ions could react with H_2O_2 to form OH and accelerate the AM dye degradation rate. The degradation mechanism of synthetic dyes by means of heterogeneous E-Fenton reactions is complex, but the first steps in the AM dye degradation in the presence of the $Fe_{3-x}Cu_xO_4$

$(0 \le x \le 0.25)$ NPs could be described by the following series of reactions [26,59,60].

$$\equiv Fe^{2+} + H_2O_2 \rightarrow \equiv Fe^{3+} + {}^{-}OH + {}^{\bullet}OH \quad (9)$$

$$\equiv Fe^{3+} + H_2O_2 \rightarrow \equiv Fe^{2+} + H^{+} + {}^{\bullet}O_2H \quad (10)$$

$${}^{\bullet}O_2H + \equiv Fe^{3+} \rightarrow \equiv Fe^{2+} + H^{+} + O_2 \quad (11)$$

$$\equiv Cu^{+} + H_2O_2 \rightarrow \equiv Cu^{2+} + {}^{-}OH + {}^{\bullet}OH \quad (12)$$

$$\equiv Cu^{2+} + O_2H \rightarrow \equiv Cu^{+} + H^{+} + O_{2(g)} \quad (13)$$

$$\equiv Cu^{2+} + {}^{\bullet}R \rightarrow \equiv Cu^{+} + R^{+} \quad (14)$$

$$\equiv Cu^{+} + \equiv Fe^{3+} \rightarrow \equiv Cu^{2+} + \equiv Fe^{2+} \quad (15)$$

where (≡) represent the surface species.

Reactions ((9)–(11)) occur on the Fe-active sites whereas reactions (13) and (14) occur on the Cu-active sites. In addition to Fe^{2+} ions (Eq. 9), the Cu^{+} ions also activate the H_2O_2 molecule forming OH and Cu^{2+} (Eq. 12). The reduction of Cu^{2+} to Cu^{+} ions can also occur through reaction with ${}^{\bullet}O_2H$ (Eq. 13) and/or by reaction with organic radical (Eq. 14). In addition, Cu^{+} ions could also react with Fe^{3+} ions and contribute to the regeneration of active Fe^{2+} sites according to equation (Eq. 15). This would correspond to a catalytic effect induced by the partial substitution of Fe^{2+} ions by Cu^{+} and Cu^{2+} ions, or to a synergic effect between Fe and Cu ions in the octahedral surface sites of the spinel structure. It should be recalled that XPS analysis showed an increase of the concentration of Cu^{2+}/Cu^{+} surface species with x, which supports the role of these ions in the activation of H_2O_2. The higher $H_2O_2/{}^{\bullet}OH$ conversion with x is then reflected in the higher kinetic of discoloration and degradation of AM dye.

3.2.2. Extent of mineralization, specific energy consumption and chemical stability of the NPs

The presence of peaks in the chromatograms other than the characteristic peak of the AM dye (Fig. SI.5A) discloses the formation of degradation by-products, which in the case of synthetic dyes are often colorless by-products or oxidized intermediate species [13,14]. However, in the present work the intensity of these peaks decreases with the increase of x, confirming the marked influence of the NPs surface composition on the efficiency of the process to oxidize organic matter. Fig. 6A shows the TOC removal values obtained during the AM dye degradation under heterogeneous E-Fenton conditions. A maximum mineralization of 12.5% was achieved after 90 min. with electrogenerated H_2O_2 only. On the other hand, the abatement of organic matter triplicated in the presence of Fe_3O_4 NPs (39% for $x = 0$) and reached 70% with the $Fe_{2.75}Cu_{0.25}O_4$ NPs. In the case of complete mineralization of the AM dye, the colorless by-products would have reacted with OH to the form CO_2, H_2O and salts.

The specific energy consumption per unit of TOC (EC/kWh kg^{-1}) associated with the oxidation of AM dye's organic matter after 90 min. of electrolysis was calculated from Eq. (16):

$$EC = \frac{i.E_{cell}.t}{1000.\Delta TOC_{(DYE)}} \quad (16)$$

where, i is the measured cell current (−2.0 A in all cases), E_{cell} the cell potential (−1.7 V in all cases), t the time of electrolysis (1.5 h) and $\Delta TOC_{(DYE)}$ the mass (kg) of removed TOC [4].

The calculated EC values for the AM dye degradation with or without the addition of the NPs were very distinct as illustrated in Fig. 6B. The EC was quite high (2712.7 kWh kg^{-1}) in the case of using electrogenerated H_2O_2 only, because of the limited mineralization of the organic matter during the process. It should be also mentioned that the by-products are oxidized more slowly than the pristine dye molecule, causing a loss efficiency and an increase

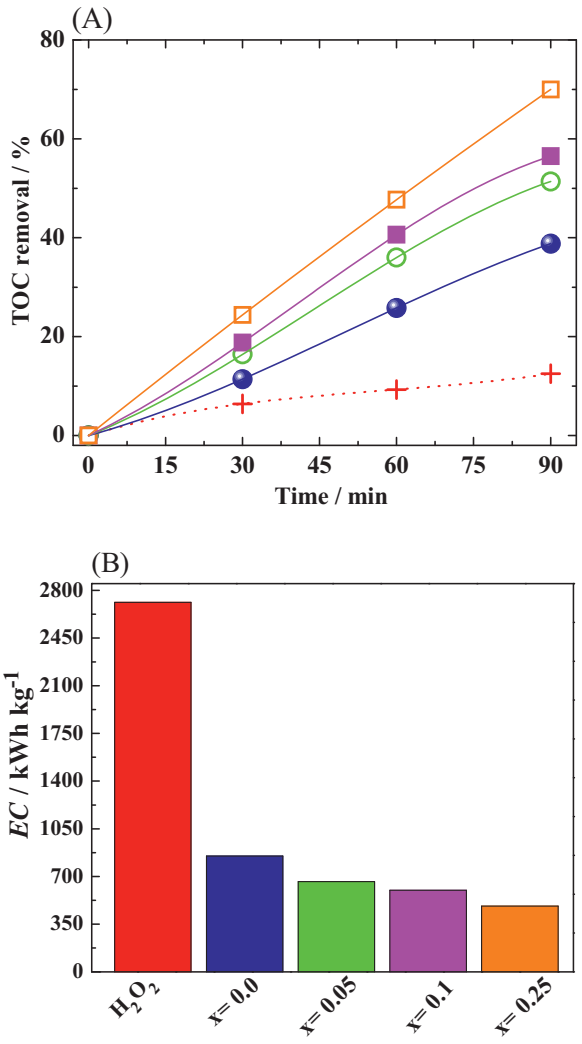

Fig. 6. (A) Total organic carbon (TOC) removal as a function of electrolysis time and (B) energy consumption (EC) after 90 min. of electrolysis using electrogenerated H_2O_2 and $Fe_{3-x}Cu_xO_4$ $(0 \le x \le 0.25)$ nanoparticles. Electrogenerated H_2O_2 (. . .+. . .), $x = 0$ (●), $x = 0.05$ (○), $x = 0.10$ (■) and x =n0.25 (□).

of the energy cost. The EC was reduced by 60% to 850 kWh kg^{-1} by using the $x = 0$ NPs, and further reduced by almost 80% to 483 kWh kg^{-1} for $Fe_{3-x}Cu_xO_4$ ($x = 0.25$) NPs. This data indicates that the AM degradation by E-Fenton in alkaline medium and in the presence of the NPs, in particular using those with $x = 0.25$, as the potential to be viable from an energetic standpoint.

Finally, the residual Fe^{2+} and Cu^{2+} ions concentrations were determined by the phenanthroline colorimetric method and EDTA-Cu^{2+} complexometric method, respectively. Accordingly, no residual Fe^{2+} and Cu^{2+} ions were detected in all cases, indicating that there was no lixiviation of the ions into the solution. A chemical Fenton experiment was carried out to verify the chemical stability of the NPs. $Fe_{2.75}Cu_{0.25}O_4$ nanoparticles (limit of solid solution and high content of both Cu and Fe) were immersed in the 1 mol L^{-1} KOH solution containing 100 mg L^{-1} of AM dye and 3370 mg L^{-1} of H_2O_2 for 90 min. under stirring as in the electrolysis cell. After NPs separation, washing and drying, XRD analysis was carried out and the diffractogram confirmed the integrity of the spinel structure (Fig. SI.6).

4. Conclusions

$Fe_{3-x}Cu_xO_4$ ($0 \leq x \leq 0.25$) NPs were tested as heterogeneous catalysts for the heterogeneous E-Fenton process in alkaline solution using an uncatalyzed GDE. The catalytic activity of the NPs was tested for the AM dye electrodegradation. It was found that the presence of the NPs in the solution improved significantly the efficiency of the process, namely with the $Fe_{2.75}Cu_{0.25}O_4$ NPs. The NPs increased the H_2O_2/•OH conversion which then promoted a higher kinetic of AM dye degradation and mineralization, and thus a lower energy consumption.

In terms of NPs composition, it was found that the AM dye degradation was enhanced by increasing the amount of copper ions in the solid solutions. This was related to the higher SSA of the NPs and to the higher surface content of Cu^{2+}/Cu^{+} ions with increasing x. It is thought that a synergic effect between Cu^{2+}/Cu^{+} and Fe^{3+}/Fe^{2+} ions is operating.

Further tests at different pHs and targeting various organic molecules with different structure and practical relevance, in addition to the reusability of the NPs, should be conducted to consolidate the potential use of these NPs in the E-Fenton process.

Acknowledgements

The authors gratefully acknowledge E. Tchoumgi Kamga (INRS-EMT) for carrying out the Fenton stability test. The authors are also greatfull for the financial support of the Brazilian Fondations: Fundação de Amparo à Pesquisa do Estado de São Paulo (FAPESP - 2011/06681-4 and 2013/06682-6) and Conselho Nacional de Desenvolvimento Científico e Tecnológico (CNPq - 301492/2013-1) and Canadian agencies: Fonds de Recherche du Québec-Nature et Technologies (FRQNT) and Centre Québécois sur les Materiaux Fonctionnels (CQMF).

Appendix A. Supplementary data

Supplementary data associated with this article can be found, in the online version, at http://dx.doi.org/10.1016/j.apcatb.2015.06.048

References

[1] R.L. Siegrist, R. Parzen, J. Tomaras, K.S. Lowe, Water Res. 52 (2014) 178–187.
[2] M. Panizza, G. Cerisola, J. Electroanal. Chem. 638 (2010) 236–240.
[3] S. Raghu, C.W. Lee, S. Chellammal, S. Palanichamy, C.A. Basha, J. Hazard. Mater. 171 (2009) 748–754.
[4] E. Brillas, I. Sirés, M.A. Oturan, Chem. Rev. 109 (2009) 6570–6631.
[5] C.A. Martínez-Huitle, E. Brillas, Appl. Catal. B 87 (2009) 105–145.
[6] Y.H. Lee, S.G. Pavlostathis, Water Res. 38 (2004) 1838–1852.
[7] Z. Aksu, Process Biochem. 40 (2005) 997–1026.
[8] Z. Aksu, S. Tezer, Process Biochem. 40 (2005) 1347–1361.
[9] L.G. Devi, S.G. Kumar, Appl. Surf. Sci. 261 (2012) 137–146.
[10] A. Adak, M. Bandyopadhyay, A. Pal, Sep. Purif. Technol. 44 (2005) 139–144.
[11] Y. Özdemir, M. Dogan, M. Alkan, Microporous Mesoporous Mater. 96 (2006) 419–427.
[12] B. Armağan, M. Turan, Desalination 170 (2004) 33–39.
[13] J.R. Steter, W.R.P. Barros, M.R.V. Lanza, A.J. Motheo, Chemosphere 117 (2014) 200–207.
[14] W.R.P. Barros, J.R. Steter, M.R.V. Lanza, A.J. Motheo, Electrochim. Acta 143 (2014) 180–187.
[15] E. Brillas, C.A. Martínez-Huitle, Appl. Catal. B 166-167 (2015) 603–604.
[16] I. Sirés, E. Brillas, M.A. Oturan, M.A. Rodrigo, M. Panizza, Environ. Sci. Pollut. Res. 21 (2014) 8336–8367.
[17] M.N. Chong, A.K. Sharma, S. Burn, C.P. Saint, J. Clean. Prod. 35 (2012) 230–238.
[18] M. Vallejo, M.F.S. Roman, I. Ortiz, A. Irabien, Chemosphere 118 (2015) 44–56.
[19] S. Garcia-Segura, F. Centellas, C. Arias, J.A. Garrido, R.M. Rodríguez, P.L. Cabot, E. Brillas, Electrochim. Acta 58 (2011) 303–311.
[20] W.R.P. Barros, P.C. Franco, J.R. Steter, R.S. Rocha, M.R.V. Lanza, J. Electroanal. Chem. 722–723 (2014) 46–53.
[21] W.R.P. Barros, S.A. Alves, P.C. Franco, J.R. Steter, R.S. Rocha, M.R.V. Lanza, J. Electrochem. Soc. 161 (2014) H438–H442.
[22] W.G. Barb, J.H. Baxendale, P. George, K.R. Hargrave, Trans. Faraday Soc. 47 (1951) 591–616.
[23] C. Walling, A. Goosen, J. Am. Chem. Soc. 95 (1973) 2987–2991.
[24] S.S. Lin, M.D. Gurol, Water Sci. Technol. 34 (1996) 57–64.
[25] S.S. Lin, M.D. Gurol, Environ. Sci. Technol. 32 (1998) 1417–1423.
[26] W.P. Kwan, B.M.M. Voelker, Environ. Sci. Technol. 37 (2003) 1150–1158.
[27] S.R. Pouran, A.A.A. Raman, W.M.A.W. Daud, J. Clean. Prod. 64 (2014) 24–35.
[28] L. Hou, Q. Zhang, F. Jérôme, D. Duprez, H. Zhanga, S. Royer, Appl. Catal. B 144 (2014) 739–749.
[29] M. Usman, P. Faure, C. Ruby, K. Hanna, Appl. Catal. B 117-118 (2012) 10–17.
[30] J.H. Choi, S.H. Kong, R.J. Watts, Chemosphere 37 (1998) 1473–1482.
[31] L. Xu, J. Wang, Appl. Catal. B 123–124 (2012) 117–126.
[32] R.C.C. Costa, F.C.C. Moura, J.D. Ardisson, J.D. Fabris, R.M. Lago, Appl. Catal. B 83 (2008) 131–139.
[33] F.C.C. Moura, M.H. Araújo, R.C.C. Costa, J.D. Fabris, J.D. Ardisson, W.A.A. Macedo, R.M. Lago, Chemosphere 60 (2005) 1118–1123.
[34] J. Chun, H. Lee, S.-H. Lee, S.-W. Hong, J. Lee, C. Lee, J. Lee, Chemosphere 89 (2012) 1230–1237.
[35] R.C.C. Costa, M.F.F. Lelis, L.C.A. Oliveira, J.D. Fabris, J.D. Ardisson, R.R.V.A. Rios, C.N. Silva, R.M. Lago, J. Hazard. Mater. 129 (2006) 171–178.
[36] R.C.C. Costa, M.F.F. Lelis, L.C.A. Oliveira, J.D. Fabris, J.D. Ardisson, R.R.V.A. Rios, C.N. Silva, R.M. Lago, Catal. Commun. 4 (2003) 525–529.
[37] F. Magalhães, M.C. Pereira, S.E.C. Botrel, J.D. Fabris, W.A. Macedo, R. Mendonça, R.M. Lago, L.C.A. Oliveira, Appl. Catal. A 332 (2007) 115–123.
[38] X. Liang, Y. Zhong, S. Zhu, L. Ma, P. Yuan, J. Zhu, H. He, Z. Jiang, J. Hazard. Mater. 199–200 (2012) 247–254.
[39] S. Yang, H. He, D. Wu, D. Chen, X. Liang, Z. Qin, M. Fan, J. Zhu, P. Yuan, Appl. Catal. B 89 (2009) 527–535.
[40] X. Zhong, Y. Liang, J. Zhong, S. Zhu, P. Zhu, H. He, J. Zhang, Water Res. 46 (2012) 4633–4644.
[41] A.C. Tavares, M.A.M. Cartaxo, M.I.S. Pereira, F.M. Costa, J. Solid State Electrochem. 5 (2001) 57–67.
[42] E. Kester, B. Gillot, P. Perriat, P. Dufour, C. Villette, P. Tailhades, A. Rousset, J. Solid State Chem. 126 (1996) 7–14.
[43] E. Kester, B. Gillot, J. Phys. Chem. Solids 59 (1998) 1259–1269.
[44] E. Kester, B. Gillot, C. Villette, P. Tailhades, A. Rousset, Thermochim. Acta 297 (1997) 71–78.
[45] M.J. Dreiling, J. Phys. Chem. Solids 37 (1976) 121–122.
[46] E. Brillas, M.A. Baños, S. Camps, C. Arias, P.-L. Cabot, J.A. Garrido, R.M. Rodríguez, New J. Chem. 28 (2004) 314–322.
[47] W.R.P. Barros, T. Ereno, A.C. Tavares, M.R.V. Lanza, ChemElectroChem 2 (2015) 714–719.
[48] W.R.P. Barros, Q. Wei, G. Zhang, S. Sun, M.R.V. Lanza, A.C. Tavares, Electrochim. Acta 62 (2015) 263–270.
[49] W.R.P. Barros, R.M. Reis, R.S. Rocha, M.R.V. Lanza, Electrochim. Acta 104 (2013) 12–18.
[50] J.C. Forti, R.S. Rocha, M.R.V. Lanza, R. Bertazzoli, J. Electroanal. Chem. 601 (2007) 63–67.
[51] American Public Health Association, Phenanthroline method/3500-Fe B, in: L.S. Eaton, E.W. Clesceri, A.E. Rice (Eds.), Standard Methods for the Examination of Water & Wastewater, 21st ed., APHA, Washington, 2005, 77(3)-79(3).
[52] R.C. Mendham, J.D. Denney, M.J.K. Barnes, Quantitative Chemical Analysis, sixth ed., Longman, UK, 2000.
[53] M. Sorescu, D.M. -Tarabasanu, L. Diamandescu, Appl. Phys. Lett. 72 (1998) 2047–2049.
[54] D.S. Mcclure, J. Phys. Chem. Solids 3 (1957) 311–317.
[55] R.D. Shannon, Acta Cryst. A 32 (1976) 751–767.
[56] D.H. Sing, R.A.W. Everett, L. Haul, R.A. Moscou, J. Pierotti, Pure Appl. Chem. 57 (57) (1985) 603–619.
[57] A.C. Tavares, M.A.M. Cartaxo, M.I.S. Pereira, F.M. Costa, J. Electroanal. Chem. 464 (1999) 187–197.
[58] A.C. Tavares, M.I.S. Pereira, M.H. Mendonça, M.R. Nunes, F.M. Costa, C.M. Sá, J. Electroanal. Chem. 449 (1998) 91–100.
[59] R. Andreozzi, V. Caprio, R. Marotta, Water Res. 36 (2002) 2761–2768.
[60] J. He, W. Ma, W. Song, J. Zhao, X. Qian, S. Zhang, J.C. Yu, Water Res. 39 (2005) 119–128.